A. Marchetti
GIAIP-CIFASIS (CONICET,UNR,UPCAM III),
27 de Febrero 210bis,
S2000EZP Rosario, Argentina

A. Gopalakrishnan
Laboratoire d' Automatique (LA),
École Polytechnique Fédérale de Lausanne
(EPFL),
CH-1015 Lausanne, Switzerland

B. Chachuat
Centre for Process Systems Engineering,
Department of Chemical Engineering,
Imperial College London, UK

D. Bonvin[1]
Laboratoire d' Automatique (LA),
École Polytechnique Fédérale de Lausanne
(EPFL),
CH-1015 Lausanne, Switzerland
e-mail: dominique.bonvin@epfl.ch

L. Tsikonis

A. Nakajo

Z. Wuillemin

J. Van herle

Laboratoire d'Énergétique Industrielle (LENI),
EPFL CH-1015 Lausanne, Switzerland

Robust Real-Time Optimization of a Solid Oxide Fuel Cell Stack

On-line control and optimization can improve the efficiency of fuel cell systems, whilst simultaneously ensuring that the operation remains within a safe region. Also, fuel cells are subject to frequent variations in their power demand. This paper investigates the real-time optimization (RTO) of a solid oxide fuel cell (SOFC) stack. An optimization problem maximizing the efficiency subject to operating constraints is defined. Due to inevitable model inaccuracies, the open-loop implementation of optimal inputs evaluated off-line may be suboptimal, or worse, infeasible. Infeasibility can be avoided by controlling the constrained quantities. However, the constraints that determine optimal operation might switch with varying power demand, thus requiring a change in the regulator structure. In this paper, a control strategy that can handle plant-model mismatch and changing constraints in the face of varying power demand is presented and illustrated. The strategy consists in the integration of RTO and model predictive control (MPC). A lumped model of the SOFC is utilized at the RTO level. The measurements are not used to re-estimate the parameters of the SOFC model at different operating points, but to simply adapt the constraints in the optimization problem. The optimal solution generated by RTO is implemented using MPC that uses a step-response model in this case. Simulation results show that near-optimality can be obtained, and constraints are respected despite model inaccuracies and large variations in the power demand. [DOI: 10.1115/1.4003976]

Keywords: fuel cells, solid oxide fuel cell stack, real-time optimization, constraint control, model predictive control

1 Introduction

Given the prohibitive cost of nonrenewable energy sources in today's scenario, fuel cells are intensively investigated as alternative power sources for a broad scope of applications. Solid oxide fuel cells (SOFCs) are energy conversion devices that produce electrical energy by the reaction of a fuel with an oxidant. Since SOFCs typically run continuously for long hours, and are subject to changes in the power demand, it is desirable to keep the performance optimal throughout, while ensuring the operation remains within safety and operability constraints [1,2]. Due to changes in the power demand during operation, and also due to external perturbations affecting the SOFC system, the set of optimal operating conditions will keep varying with time. Hence, there is a need for real-time optimization, i.e., regular adjustment of the operating variables (e.g., flow rates, electric current) to maximize the performance (e.g., power output, efficiency) of the fuel cell.

Different approaches have been proposed in the literature for controlling fuel cells. Aguiar et al. [3] discussed the use of PID feedback control in the presence of power load changes. For the case of a proton exchange membrane (PEM) fuel cell, Golbert and Lewin [2,4] used a nonlinear MPC scheme with a target function that attempts to simultaneously track changes in the power setpoint and maximize efficiency. Recently, Zhang et al. [1] applied nonlinear MPC to a planar SOFC. However, these authors consider a square control problem, i.e., without residual degrees of freedom available for optimization. Several other control strategies for fuel cells have also been reported in the literature [5–7].

RTO is typically a nonlinear program (NLP) minimizing cost or maximizing economic productivity subject to constraints. The underlying model is derived from steady-state mass and energy balances and physical relationships. RTO is typically located at the higher level of a two-level cascade structure. Then, at the lower level, the control system implements the RTO results [8]. MPC is a natural choice for this task because of its ability to handle large multivariable control problems and to accommodate input bounds and process constraints. While originally developed for oil refineries and power plants, the MPC technology is now used in a wide variety of applications [9]. Recently, it has also been proposed for the control of fuel cells [1,4].

Because accurate mathematical models are unavailable for most industrial applications, RTO classically proceeds via a two-step approach, namely, a parameter estimation step followed by an optimization step. Parameter estimation is complicated by several factors: (i) the complexity of the models and the nonconvexity of the parameter estimation problems and (ii) the need for model parameters to be identifiable from the available measurements. Moreover, in the presence of structural plant-model mismatch, parameter estimation does not necessarily lead to improved operation since matching the plant outputs does not imply that their gradient with respect to the inputs will be matched as well [10].

The constraint-adaptation approach used in this paper avoids the task of updating the model parameters on-line. Based on the observation that, for a large number of optimization problems, most of the optimization potential arises from operating the plant

[1]Corresponding author.

Contributed by the Advanced Energy Systems Division of ASME for publication in the JOURNAL OF FUEL CELL SCIENCE AND TECHNOLOGY. Manuscript received May 14, 2009; final manuscript received January 28, 2011; published online June 13, 2011. Editor: Nigel M. Sammes.

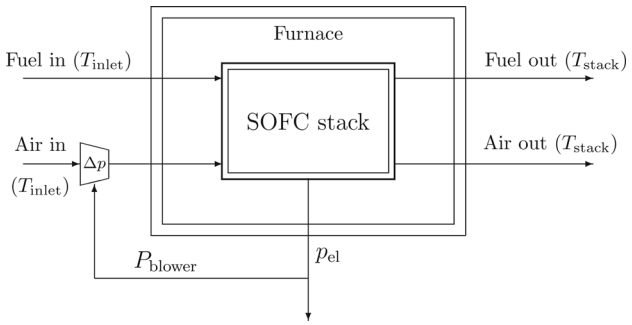

Fig. 1 Schematic of the SOFC stack and furnace

at some of the constraints [11,12], constraint-adaptation schemes have been developed to use appropriate measurements and adjust the constraint functions in the RTO problem [12,13].

Constraint adaptation guarantees to reach a feasible operating point upon convergence, that is, a point that satisfies all the constraints. However, the iterates may follow an infeasible path, even when adaptation is started from within the feasible region. Process disturbances and changes in the power demand may also result in constraint violation. Hence, MPC should implement the RTO results while avoiding constraint violations. The approach for integrating RTO with MPC described in this paper places high emphasis on how the constraints are handled.

The paper is organized as follows. The SOFC system and its mathematical model are described in Sec. 2. Section 3 formulates the optimization problem and presents the nominal solution. The constraint-adaptation approach to RTO is described and applied to the SOFC system in Sec. 4. The strategy combining constraint adaptation and constraint control via MPC is implemented in Sec. 5. Finally, Sec. 6 concludes the paper.

2 Model of SOFC System

The process is represented schematically in Fig. 1. It comprises a five-cell S-design planar SOFC stack operating in an electrically heated furnace [14]. The stack is fueled with H_2 humidified with 3% molar fraction of water. Only the electrochemical oxidation reaction between H_2 and O_2 is considered. The furnace temperature is constant at 780 °C. The gas temperatures at the entrance of the stack are constant at 750 °C. A blower outside the furnace delivers air to the cathode, whereas the fuel is provided directly at the desired pressure and flow rate.

2.1 Dynamic Model. A lumped model is used, as it captures the fundamental behavior of the SOFC while providing a good trade-off between accuracy and fast computation. The model has been validated from more detailed models developed at LENI-EPFL, and it corresponds to SOFC stacks typically running at LENI's facilities [15,16]. The model comprises energy equations, mole balances and electrochemical balances at the anode and cathode. The nomenclature used is given in the SOFC model nomenclature section, and the parameter values are given in Table 1.

Table 1 Parameter values

Kinetic parameters					
$E_{act,cath}$	1.53×10^5	J/mol	$k_{0,cath}$	4.10×10^{11}	$1/\Omega m^2$
E_{elect}	7.62×10^4	J/mol	$\sigma_{0,elect}$	1.63×10^4	$1/\Omega m^2$
$R_{0,cath}$	0.92×10^{-13}	Ωm^2	$E_{diss,cath}$	1.49×10^5	J/mol
Cell properties					
A_{active}	5×10^{-3}	m^2	A_{stack}	4.69×10^{-2}	m^2
m_{stack}	2.647	kg	$(mc_p)_{stack}$	2.33×10^2	J/kg K
N_{cell}	5		FU_{adj}	0.15	
$\mathcal{F}$	0.667				

2.1.1 Energy Balance. The fuel and the oxidant (air) that enter the stack react electrochemically, releasing heat and electrical power. The energy balance for the stack is

$$(mc_p)_{stack}\frac{dT_{stack}}{dt} = -\Delta\dot{H}_{gases} - P_{el} - \dot{Q}_{loss} \tag{1}$$

where the electrical power is given by

$$P_{el} = U_{cell}N_{cell}I \tag{2}$$

Only radiative heat loss from the stack is taken into account

$$\dot{Q}_{loss} = A_{stack}\mathcal{F}\sigma_{SB}\left(T_{stack}^4 - T_{furnace}^4\right) \tag{3}$$

where $\mathcal{F}$ is the transfer factor for radiative heat exchange between the stack and the furnace calculated for the case of a body enclosed into another [17].

2.1.2 Mole Balance. The mole balances consider the species H_2O and H_2 at the anode and O_2 and N_2 at the cathode. The only reaction taking place is the electrochemical oxidation of H_2, for which the overall reaction is

$$H_2 + \frac{1}{2}O_2 \rightarrow H_2O$$

From Faraday's law, the amount of H_2 participating in the reaction is related to the current produced in the reaction

$$\dot{n}_{H_2,reac} = \frac{IN_{cell}}{2F} \tag{4}$$

The mole balances at the anode and cathode give

$$\dot{n}_{i,an,out} = \dot{n}_{i,an,in} + \nu_i\,\dot{n}_{H_2,reac}, \quad i = \{H_2,\ H_2O\} \tag{5}$$

$$\dot{n}_{j,cath,out} = \dot{n}_{j,cath,in} + \nu_j\,\dot{n}_{H_2,reac}, \quad j = \{O_2,\ N_2\} \tag{6}$$

where ν_i is the stoichiometric coefficient of component i in the reaction

2.1.3 Electrochemical Model. The electrochemical model computes the cell potential and average current density as a function of the operating conditions, i.e., temperature, flow rates and gas compositions. The reversible cell voltage U_{Nernst} is computed from the change in Gibbs free enthalpy for the H_2 oxidation reaction as

$$U_{Nernst} = \frac{-\Delta G_{reaction}}{n_e F} \tag{7}$$

This is the maximal amount of potential that can be delivered by the cell. The actual voltage is subject to overpotentials due to losses appearing during operation. The losses considered here include: ohmic losses due to the ionic resistance of the electrolyte and current collectors, activation losses due to charge transfer kinetics, diffusion losses due to concentration gradients between the electrode surface and the bulk flow, and losses due to the dissociation of the oxygen molecules into ions on the cathode surface. The effective cell potential U_{cell} is given by

$$U_{cell} = U_{Nernst} - \eta_{act,cath} - \eta_{ionic,elect} - \eta_{diss,cath} - \eta_{diff,an} - \eta_{diff,cath} \tag{8}$$

The cathode activation overpotential is expressed by the Butler–Volmer equation [18]

$$\eta_{act,cath} = \frac{RT_{stack}}{F}\sinh^{-1}\left(\frac{i}{2i_{0,cath}}\right) \tag{9}$$

Table 2 Fixed operating conditions

Fuel feed composition	3% H_2O, 97% H_2	T_{in} (fuel and air)	750 °C
Air feed composition	21% O_2, 79% N_2	$T_{furnace}$	780 °C

$$i_{0,\text{cath}} = \frac{2RT_{\text{stack}}}{F} k_{0,\text{cath}} \exp\left(\frac{-E_{\text{act,cath}}}{RT_{\text{stack}}}\right) \tag{10}$$

The anode overpotential is relatively small and is neglected. The Ohmic overpotential is expressed as [19]

$$\eta_{\text{ionic,elect}} = i\left(\frac{h_{\text{elect}}}{\sigma_{\text{ionic,elect}}}\right) \tag{11}$$

$$\sigma_{\text{ionic,elect}} = \sigma_{0,\text{elect}} \exp\left(\frac{-E_{\text{elect}}}{RT_{\text{stack}}}\right) \tag{12}$$

The concentration overpotential in the anode is calculated as

$$\eta_{\text{diff,an}} = -\frac{RT_{\text{stack}}}{2F} \ln\left[1 - (FU + FU_{\text{adj}})\right] \tag{13}$$

$$\text{FU} = \frac{\dot{n}_{\text{H}_2,\text{reac}}}{\dot{n}_{\text{H}_2,\text{an,in}}} \tag{14}$$

where FU is the fuel utilization factor, defined as the ratio of amount of H_2 consumed to the amount of H_2 at the inlet. FU_{adj} is an adjustment factor. The concentration overpotential in the cathode is calculated as

$$\eta_{\text{diff,cath}} = -\frac{RT_{\text{stack}}}{2F} \ln\left(1 - \frac{\text{FU}}{\lambda_{\text{air}}}\right) \tag{15}$$

$$\lambda_{\text{air}} = \frac{2\dot{n}_{\text{O}_2,\text{cath,in}}}{\dot{n}_{\text{H}_2,\text{an,in}}} \tag{16}$$

where λ_{air} is the excess air ratio, defined as the amount of oxygen to hydrogen in the feed over the stoichiometric ratio.

The overpotential loss due to the dissociation of oxygen at the cathode is

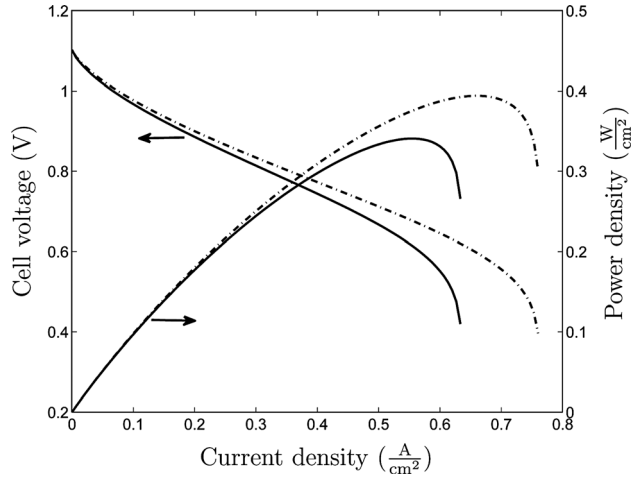

Fig. 2 Cell voltage and power density as a function of current density. Solid lines: $\dot{n}_{\text{fuel,in}} = 10^{-3}$ mol/s; dot-dashed lines: $\dot{n}_{\text{fuel,in}} = 1.2 \times 10^{-3}$ mol/s.

$$\eta_{\text{diss,cath}} = R_{0,\text{cath}} \left(\frac{p_{\text{O}_2,\text{in}}}{p_0}\right)^{-0.5} \exp\left(\frac{E_{\text{diss,cath}}}{RT_{\text{stack}}}\right) i \tag{17}$$

The operating conditions are listed in Table 2.

2.2 Performance Curves. A plot of cell voltage and power density as a function of the current density is shown in Fig. 2 for fuel inlet flow rates of 10^{-3} mol/s (or mass flow density of 6 ml/min cm^2) and 1.2×10^{-3} mol/s (7.2 ml/min cm^2), and an excess air ratio $\lambda_{air} = 3$.

At $\dot{n}_{\text{fuel,in}} = 10^{-3}$ mol/s, the limiting current density is 0.64 A/cm^2. The maximal power density at which the cell can operate is 0.35 W/cm^2. Increasing the current further would result in a sharp drop in power due to an increase in overpotential losses. To deliver more power, it is necessary to increase the fuel inlet flow rate. At $\dot{n}_{\text{fuel,in}} = 1.2 \times 10^{-4}$ mol/s, it is possible to reach power densities of up to 0.4 W/cm^2.

3 Optimization Problem

3.1 Problem Formulation. The objective of RTO is the optimization of some steady-state operating performance (e.g., minimization of operating cost or maximization of efficiency), while satisfying a number of constraints (e.g., bounds on process variables or product specifications). In the context of RTO, since it is important to distinguish between the plant and the model, we will use the notation $(\cdots)_p$ for the variables associated with the plant.

The steady-state optimization problem for the plant can be formulated as follows [12]

$$\begin{aligned} \min_{\mathbf{u}} \Phi_p(\mathbf{u}) &:= \phi(\mathbf{u}, \mathbf{y}_p) \\ \text{s.t. } \mathbf{H}_p(\mathbf{u}) &:= \mathbf{h}(\mathbf{u}, \mathbf{y}_p) = \mathbf{H}^S \\ \mathbf{G}_p(\mathbf{u}) &:= \mathbf{g}(\mathbf{u}, \mathbf{y}_p) \le \mathbf{G}^U \end{aligned} \tag{18}$$

where $\mathbf{u} \in \mathbb{R}^{n_u}$ denotes the decision (or input) variables,[2] and $\mathbf{y}_p \in \mathbb{R}^{n_y}$ are the measured (or output) variables; ϕ is the scalar objective function to be minimized; $\mathbf{h} \in \mathbb{R}^{n_h}$ are the equality constraint functions for which $\mathbf{H}^S$ represent the setpoint values; $\mathbf{g} \in \mathbb{R}^{n_g}$ are the inequality constraint functions for which $\mathbf{G}^U$ represent the upper bounds. These inequality constraints include input bounds. Also, it is assumed throughout that ϕ, $\mathbf{h}$ and $\mathbf{g}$ are known functions of $\mathbf{u}$ and $\mathbf{y}$, i.e., they can be evaluated directly from the measurements.

3.1.1 Input and Output Variables. In the case of the SOFC system considered here, there are three degrees of freedom that can be specified as input variables: the molar fuel flow rate at the anode, the molar air flow rate at the cathode, and the current:

$$\mathbf{u} = \left[\dot{n}_{\text{fuel,in}},\ \dot{n}_{\text{air,in}},\ I\right]^T \tag{19}$$

The output variables are the stack temperature, the cell potential, and the generated electric power:

$$\mathbf{y}_p = \left[T_{\text{stack}},\ U_{\text{cell}},\ P_{\text{el}}\right]^T \tag{20}$$

3.1.2 Objective Function and Constraints. The objective function to maximize is the electrical efficiency of the fuel cell for a given power demand, subject to operational constraints. Electrical efficiency is defined as the fraction of chemical power converted into useful power. Not all the power generated by the fuel cell is available for use. Due to pressure loss along the air channel,

[2]The notation $\mathbf{x} \in \mathbb{R}^n$ is used to indicate that $\mathbf{x}$ is an n-dimensional vector of real variables.

Table 3 Values of constraint bounds (L: lower, U: upper)

T^L_{stack}	730	°C	T^U_{stack}	800	°C
U^L_{cell}	0.7	V	FU^U	70	%
λ^L_{air}	3		λ^U_{air}	7	
$\dot{n}^L_{\text{fuel, in}}$	5×10^{-4}	mol/s	i^U	0.6	A/cm^2

Table 4 Values of the uncertain parameters for the plant and the nominal model

Parameter	Plant	Nominal model
$E_{\text{act, cath}}$ (J/mol)	1.53×10^5	1.5×10^5
$k_{0,\text{cath}}$ ($1/\Omega\,\text{m}^2$)	4.10×10^{11}	4.5×10^{11}
$R_{0,\text{cath}}$ ($\Omega\,\text{m}^2$)	0.92×10^{-13}	10^{-13}

some power is used internally by the blower to pump air. This power is the product of the pressure loss along the air channel and the volumetric flow rate of air. Hence, the electrical efficiency to maximize is

$$\eta = \frac{P_{\text{el}} - P_{\text{blower}}}{\dot{n}_{\text{H}_2,\text{an,in}}\text{LHV}} = \frac{U_{\text{cell}} I N_{\text{cell}} - \Delta p \dot{Q}_{\text{air}}/\eta_{\text{blower}}}{\dot{n}_{\text{H}_2,\text{an,in}}\text{LHV}} \tag{21}$$

where the efficiency of the blower is $\eta_{\text{blower}} = 0.4$, and the pressure loss along the air channel Δp is proportional to the flow rate of air. LHV is the lower heating value of the fuel, which is the amount of heat released by burning a specific quantity of fuel.

The fuel cell is operated under a number of inequality constraints including bounds on input and output variables. Limitations on the potential and fuel utilization are set due to risks of oxidation of the anode, which may degrade or even cause the failure of the cell [15,18]. Operating at high current densities will cause material damage to the cell through excessive heating [20]. The low air-ratio limit is set to avoid high thermal gradients, whilst the high limit is due to system constraints. Current density is constrained to avoid degradation [15,20]. The constraint bounds are given in Table 3. The setpoint value p^S_{el} for the produced power density is specified as an equality constraint.

The optimization problem can be formulated mathematically as follows

$$\begin{aligned} \max_{\dot{n}_{\text{fuel, in}}, \dot{n}_{\text{air, in}}, I} \quad & \Phi = \eta \\ \text{s.t.} \quad & H: p_{\text{el}} = p^S_{\text{el}} \\ & G_1: T_{\text{stack}} \le T^U_{\text{stack}}, \quad G_2: T_{\text{stack}} \ge T^L_{\text{stack}} \\ & G_3: U_{\text{cell}} \ge U^L_{\text{cell}}, \quad G_4: \text{FU} \le \text{FU}^U \\ & G_5: \lambda_{\text{air}} \le \lambda^U_{\text{air}}, \quad G_6: \lambda_{\text{air}} \ge \lambda^L_{\text{air}} \\ & G_7: \dot{n}_{\text{fuel, in}} \ge \dot{n}^L_{\text{fuel, in}}, \quad G_8: i \le i^U \end{aligned} \tag{22}$$

Because the current density i and the power density p_{el} are not actually measured, they are considered to be proportional to the current I, namely, $i = I/A_{\text{active}}$, and the power P_{el}, namely, $p_{\text{el}} = P_{\text{el}}/A_{\text{active}}$. Hence, the constraint G_8 represents an input bound on the current.

3.2 Nominal Optimization. In any practical application, the plant mapping $\mathbf{y}_p(\mathbf{u})$ is not known accurately. However, an approximate model is often available in the form

$$\begin{aligned} \mathbf{f}(\mathbf{u}, \mathbf{x}, \theta) &= \mathbf{0} \\ \mathbf{y} &= \mathcal{H}(\mathbf{u}, \mathbf{x}, \theta) \end{aligned}$$

where $\mathbf{f} \in \mathbb{R}^{n_x}$ is a set of process model equations including mass and energy balances and thermodynamic relationships, $x \in \mathbb{R}^{n_x}$ are the state variables, $y \in \mathbb{R}^{n_y}$ are the output variables predicted by the model, and $\theta \in \mathbb{R}^{n_\theta}$ is a set of adjustable model parameters. Using one such model, the solution of the original problem (18) can be approached by solving the following nonlinear programming (NLP) problem

$$\begin{aligned} \min_{\mathbf{u}} \Phi(\mathbf{u}, \theta) &:= \phi(\mathbf{u}, \mathbf{y}(\mathbf{u}, \theta)) \\ \text{s.t. } \mathbf{H}(\mathbf{u}, \theta) &:= \mathbf{h}(\mathbf{u}, \mathbf{y}(\mathbf{u}, \theta)) = \mathbf{H}^S \\ \mathbf{G}(\mathbf{u}, \theta) &:= \mathbf{g}(\mathbf{u}, \mathbf{y}(\mathbf{u}, \theta)) \le \mathbf{G}^U \end{aligned} \tag{23}$$

Assuming that the feasible set $U := \{\mathbf{u} : \mathbf{H}(\mathbf{u}, \theta) = \mathbf{H}^S; \mathbf{G}(\mathbf{u}, \theta) \le \mathbf{G}^U\}$ is nonempty and compact for θ given, and that $\Phi(\mathbf{u}, \theta)$ is continuous on U, a minimizing solution, $\mathbf{u}^*$, of problem (23) is guaranteed to exist. Furthermore, the set of active inequality constraints at u^* is denoted by $\mathcal{A} := \{i : G_i(\mathbf{u}^*, \theta) = 0,\ i = 1, \ldots, n_g\}$.

3.3 Effect of Plant-Model Mismatch. In this simulation work, plant-model mismatch is considered by modifying certain model parameters. The uncertain parameters are given in Table 4 with the values for both the plant (simulated reality) and the nominal model.

Contour maps showing the objective function and the constraints at steady state as functions of the input variables for different power density setpoints are presented in Fig. 3 for the plant (simulated reality). These plots show the location of the plant optimum (point P) and the constraint bounds. Since the power density is set and the active cell area is given, the power P_{el} is fixed, which determines the current as $I = P_{\text{el}}/(U_{\text{cell}} N_{\text{cell}})$. Hence, the input space is only two-dimensional, and it is spanned by the air and fuel flow rates.

The set of active constraints at the optimum may change with the requested power density. At the power density of 0.2 W/cm^2, the optimum lies on the upper bound on fuel utilization (FU). The efficiency is about 40%. As the power setpoint is increased, the active constraint switches to the constraint on the cell potential, and it is not possible to reach the maximal FU. The optimal efficiency therefore drops. At a higher power density (0.45 W/cm^2), the active constraint is the current density, and the optimal operating point gives around 21% efficiency.

Similar contour maps can be drawn for the nominal model (Fig. 4). Point M indicates the location of the model optimum. The constraints predicted by the model are different from those of the plant. It is also possible that, for the same power density setpoint, the set of active constraints at the optimum are different for the nominal model and the plant. For example, at the power density of 0.3 W/cm^2, the active constraint for the plant is on the cell potential, whereas both the cell potential and the fuel utilization constraints are active for the model. Even more different, at the power density of 0.45 W/cm^2, the plant optimum is at the intersection of the lower bound on λ_{air} and the upper bound on the current density, whereas the lower bound on λ_{air} is not active for the nominal model.

4 RTO Via Constraint Adaptation

4.1 Constraint-Adaptation Scheme. In the presence of uncertainty such as plant-model mismatch or process disturbances, the constraint values predicted by the model do not quite match those of the plant. The idea behind constraint adaptation is to use measurements for correcting the constraint predictions between successive RTO iterations so as to track the actual plant

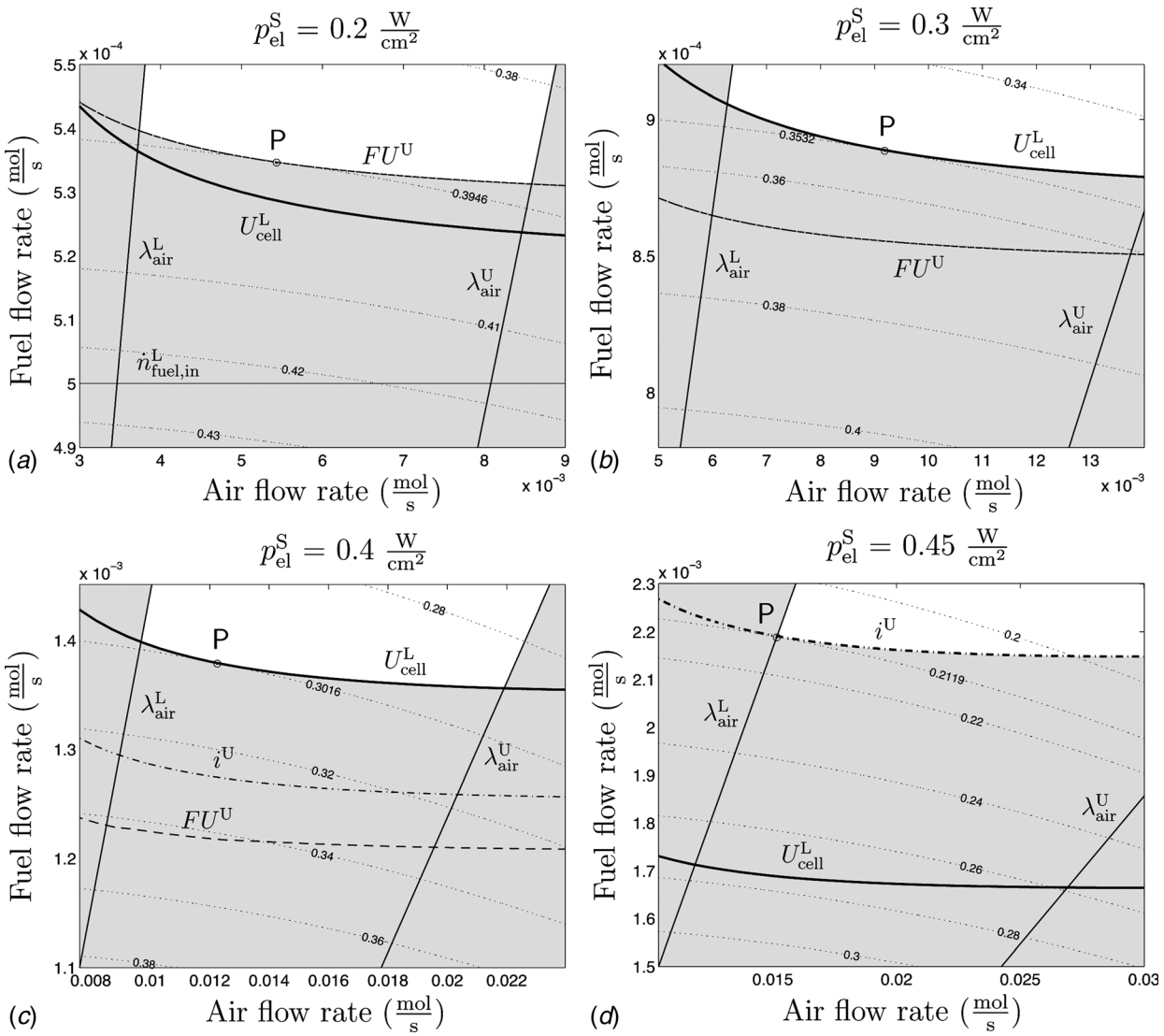

Fig. 3 Contour maps and operational constraints for the plant at steady state corresponding to different power density setpoints. White area: feasible region; dotted lines: contours of the objective function; point P: optimum for the plant.

constraints [12,13]. Such a correction can be made by simply offsetting the constraint predictions as

$$\mathbf{H}(\mathbf{u},\,\theta) + \varepsilon^H = \mathbf{H}^S \tag{24}$$

$$\mathbf{G}(\mathbf{u},\,\theta) + \varepsilon^G \le \mathbf{G}^U \tag{25}$$

where $\varepsilon^H \in \mathbb{R}^{n_h}$ are the equality constraint modifiers and $\varepsilon^G \in \mathbb{R}^{n_g}$ the inequality constraint modifiers.

The decision variables are updated at each RTO iteration by solving an NLP problem similar to Eq. (23), which takes the constraint modifiers into account. At the kth iteration, the next optimal input values are computed:

$$\begin{aligned}\mathbf{u}_{k+1}^* = \arg\min_{\mathbf{u}}\ & \Phi(\mathbf{u},\theta)\\ \text{s.t. } & \mathbf{H}(\mathbf{u},\theta) + \varepsilon_k^H = \mathbf{H}^S\\ & \mathbf{G}(\mathbf{u},\theta) + \varepsilon_k^G \le \mathbf{G}^U\end{aligned} \tag{26}$$

where ε_k^H and ε_k^G are the constraint modifiers at the current iteration. If constraint adaptation alone is applied, the new operating point is obtained by applying the optimal inputs directly to the plant

$$\mathbf{u}_{k+1} := \mathbf{u}_{k+1}^* \tag{27}$$

However, if constraint adaptation is combined with MPC, as will be described in Sec. 5, the real inputs are determined by the controller, and the values $\mathbf{u}_{k+1}$ to be used in the next RTO iteration correspond to those real inputs.

Assuming that all constrained quantities can be measured at steady state, the constraint modifiers can be updated for the next RTO iteration as follows:

$$\varepsilon_{k+1}^H = \mathbf{H}_p(\mathbf{u}_{k+1}) - \mathbf{H}(\mathbf{u}_{k+1},\,\theta) \tag{28}$$

$$\varepsilon_{k+1}^G = \mathbf{G}_p(\mathbf{u}_{k+1}) - \mathbf{G}(\mathbf{u}_{k+1},\theta) \tag{29}$$

On the other hand, the model parameters θ are not subject to adaptation

The constraint-adaptation algorithm is illustrated in Fig. 5. The approach relies on constraint measurements only, and it does not require that gradients be estimated. However, since the model gradients do not quite match the plant gradients, the constraint-adaptation algorithm may terminate at a suboptimal, yet feasible, point upon convergence. This loss of optimality depends on the quality of the process model used in the numerical optimization step.

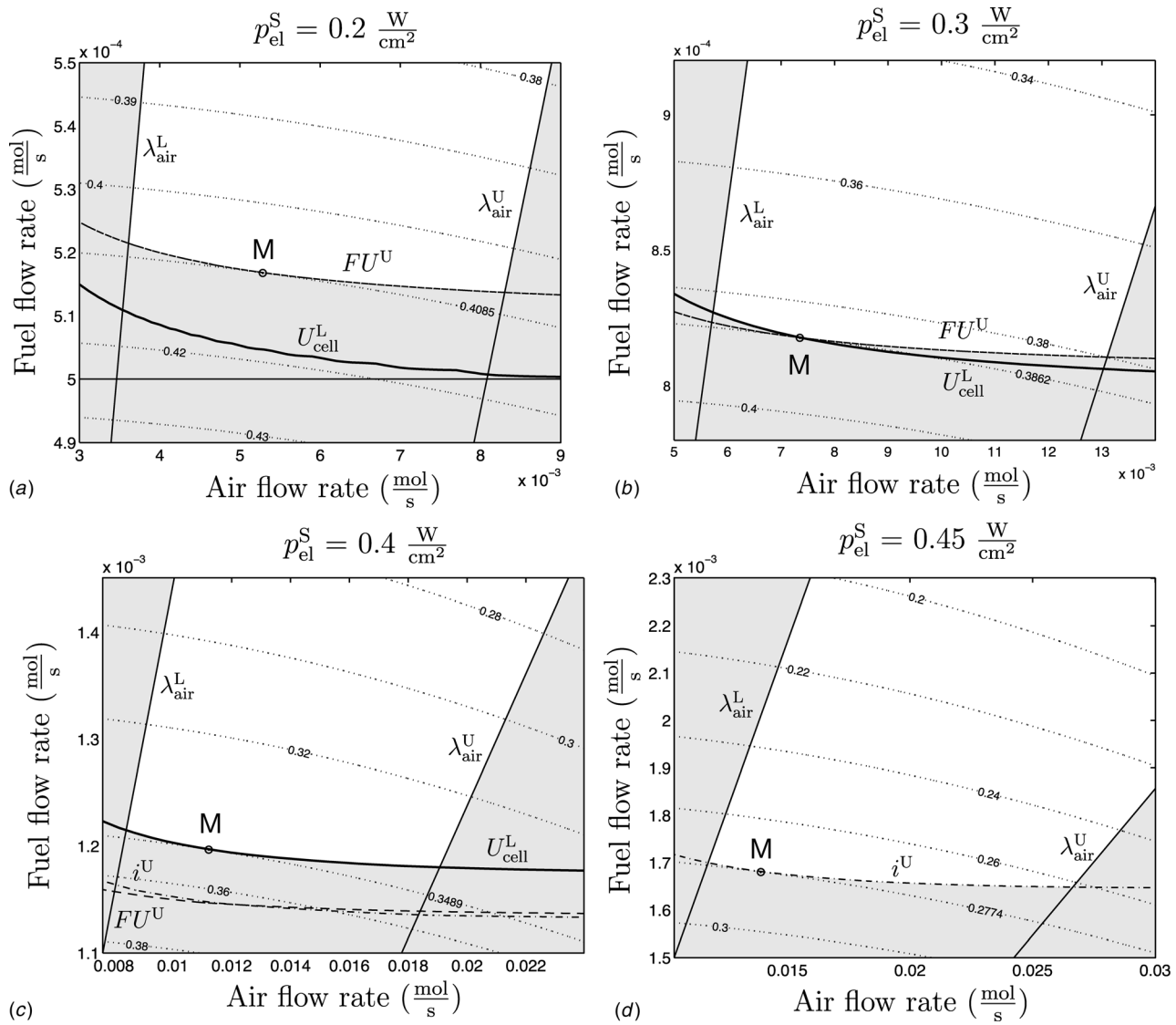

Fig. 4 Contour maps and operational constraints for the nominal model at steady-state corresponding to different power density setpoints. White area: feasible region; dotted lines: contours of the objective function; point M: optimum for the model.

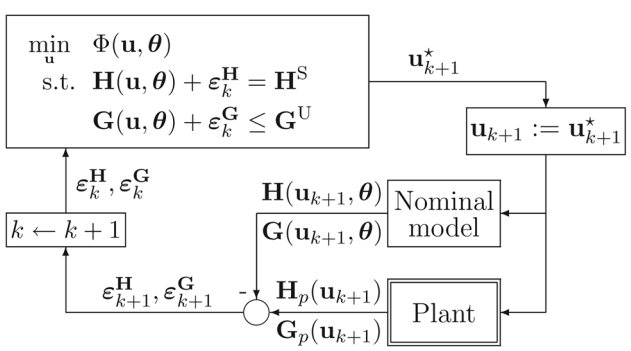

Fig. 5 Constraint-adaptation algorithm for real-time optimization. The subscript *k* represents the iteration counter. The constrained quantities H, G, H_p, and G_p correspond to steady-state operation. When implemented alone, i.e., without an additional controller, the optimal inputs $\mathbf{u}_{k+1}^\star$ are applied directly to the plant as indicated in this figure; otherwise, the process inputs are determined by the controller as detailed in Sec. 5.

4.2 Application to SOFC System. The time constant of the fuel cell is around 40 s. A RTO period of 10 min is chosen, which leaves sufficient time for the system to reach steady state following an input change. The constraint-adaptation scheme is applied using the parameter values of Table 4 for the plant and the nominal model. The nominal model corresponds to a steady-state model, i.e., with $dT_{stack}/dt = 0$ in Eq. (1). Figure 6 shows the response of some of the key variables. Initially, the plant is at steady-state with the power density setpoint $p_{el}^S = 0.4\ W/cm^2$ and the corresponding inputs $\mathbf{u}_0 = [1.9 \times 10^{-3},\ 14 \times 10^{-3},\ 26.0]^T$. Constraint adaptation is started at $t = 10$ min. Since the system is not optimized up to $t = 10$ min, the efficiency is low in this period. Although we start at a feasible operating point, the algorithm overestimates the adaptation of U_{cell} in the first RTO iteration. This results in a slight violation of the constraint between 10 and 20 min. Convergence is practically reached at the second iteration. At time $t = 40$ min, the setpoint is changed to $p_{el}^S = 0.2\ W/cm^2$. As a result, the fuel and air flow rates and the current are reduced, and efficiency goes up. The active constraint is now FU. This constraint is not violated since it depends only on the input variables that are not subject to plant-model mismatch. At $t = 70$ min, the setpoint is changed back to $p_{el}^S = 0.4\ W/cm^2$ and, again, there is violation of the U_{cell} constraint.

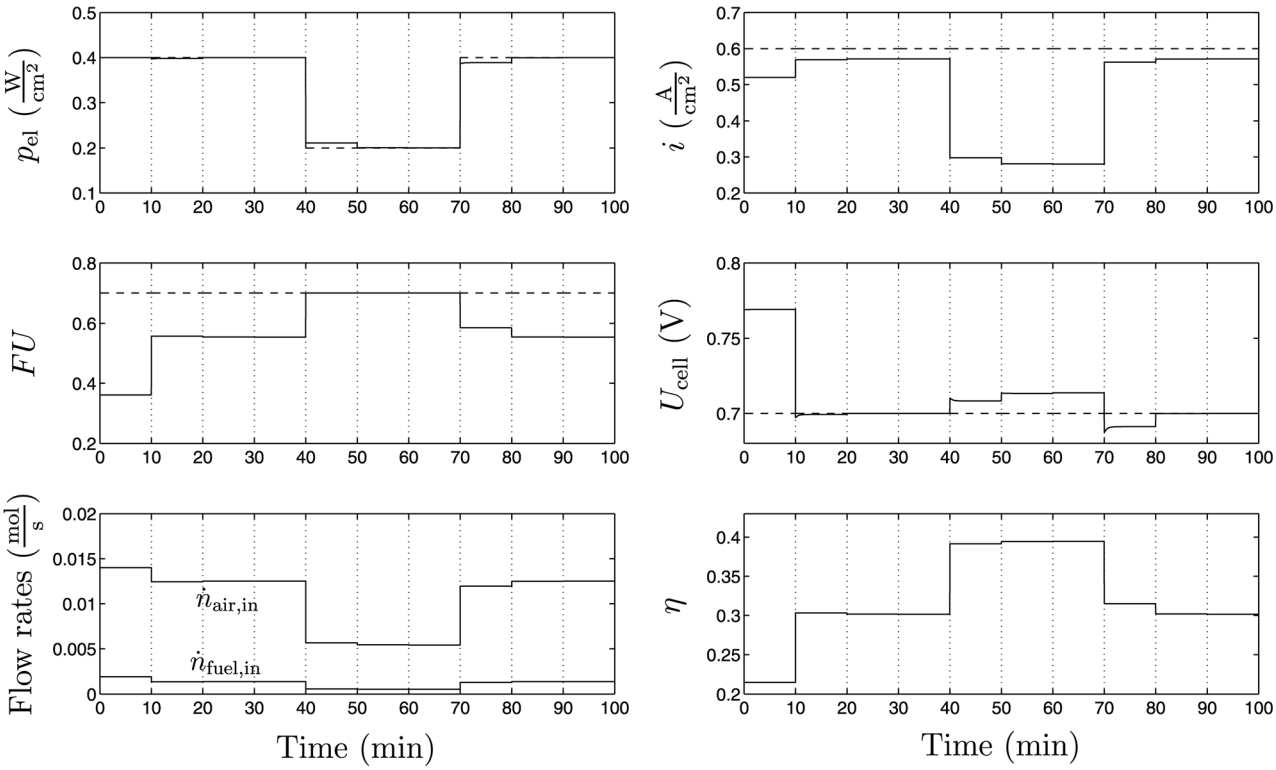

Fig. 6 Real-time optimization of the SOFC stack. Solid lines: Constraint-adaptation results. Dashed lines: Power density set-point and constraint bounds. The three inputs are the flow rates $\dot{n}_{\mathrm{fuel,\,in}}$ and $\dot{n}_{\mathrm{air,\,in}}$, and the current $I = A_{\mathrm{active}}\, i$.

4.3 Accuracy of Constraint Adaptation. The accuracy of the constraint-adaptation scheme upon convergence is illustrated in Table 5. The performance loss, η_{loss}, is computed as

$$\eta_{\mathrm{loss}} = \frac{\eta_p^* - \eta_\infty^*}{\eta_p^*} \tag{30}$$

where η_p^* is the true optimal efficiency of the plant, and η_∞^* is the objective function value obtained upon convergence of the constraint-adapation scheme. This optimality loss is negligible in spite of the presence of model mismatch.

5 Robust RTO via Adaptation and Control of the Constraints

5.1 Enforcing Constraints via MPC. Constraint adaptation guarantees to reach a feasible operating point upon convergence. However, in the presence of modeling errors and process disturbances, constraint adaptation does not ensure feasibility prior to convergence. An additional complication is given by the fact that, in the presence of process disturbances and changing operating conditions, the set of active inequality constraints may change, thus requiring a change in the regulation structure of the plant [11,21]. Yet, constraint violations can be prevented by controlling all the constrained quantities.

The equality constraints $\mathbf{H}$ are controlled at their setpoint values $\mathbf{H}^S$. Between the RTO iterations k and $k+1$, the subset $\mathrm{G}_{c_k} \in \mathbb{R}^{n_{c_k}}$ of the inequality constraints $\mathbf{G}$ are controlled at the setpoints $\mathbf{G}_{c_k}^S := \mathbf{G}_{c_k}(\mathbf{u}_{k+1}^*, \theta) + \varepsilon_{c_k}^G$.[3] The controlled constraints $\mathbf{G}_{c_k}$ can be selected as the active inequality constraints at the kth RTO iteration, thus leading to $\mathbf{G}_{c_k}^S = \mathbf{G}_{c_k}^U$. However, inactive constraints can be selected as well, as long as $n_{c_k} \leq (n_u - n_h)$ to avoid over-specification. In practice, input-output selection criteria should also guide the selection of the inequality constraints to be included in $\mathbf{G}_{c_k}$. For example, consider the optimal operating point predicted by the model for the case of Fig. 4(b). The optimum is at the intersection of the cell potential and the fuel utilization constraints. However, because of the near collinearity between these two constraints, if both of them were selected as controlled variables, the controlled plant would become ill-conditioned and very sensitive to process disturbances.

The methodology for combining constraint adaptation and constraint control is presented next. Constraint control is implemented using dynamic matrix control (DMC), which is one of the original MPC formulations, and still one of the most popular MPC algorithms in industry [22]. DMC uses a step response model of truncation order n. However, other prediction models could be used as well. Using MPC, constraint control can be implemented between the RTO iterations k and $k+1$ by minimizing the quadratic objective function

$$J_k[\mathbf{u}(t)] = \sum_{l=1}^{p} \left\| D_l \left[\mathbf{H}(t+l|t) - \mathbf{H}^S \right] \right\|^2 + \left\| Q_{l,k} \left[\mathbf{G}_{c_k}(t+l|t) - \mathbf{G}_{c_k}^S \right] \right\|^2 + \left\| R_l \Delta \mathbf{u}(t+l-1) \right\|^2 \tag{31}$$

where D_l is the weighting matrix on the equality constraints, $\mathrm{Q}_{l,k}$ the weighting matrix on the controlled inequality constraints, and R_l the weighting matrix on the rate of change of the inputs.

At current time t, the behavior of the process over p future time steps is considered. MPC determines the next m input moves $\Delta \mathbf{u}(t+l|t) := \mathbf{u}(t+l|t) - \mathbf{u}(t+l-1|t), \quad l = 0, \ldots, m-1,$ with $m < p$ and $\Delta \mathbf{u}(t+l|t) = \mathbf{0}, \ \forall l \geq m$. Only the first computed change in the manipulated variables is implemented, and at time $t+1$ the computation is repeated with the horizon moved by one time interval. Implementation details can be found in Ref. [23].

[3]The notation requires some explanation. Here, ε_k^G are the correction terms given by Eq. (35), and $\varepsilon_{c_k}^G$ is the subset of ε_k^G corresponding to the inequality constraints that are controlled between the RTO iterations k and $k+1$. Notice that the controlled inequality constraints might change from one iteration to the next, hence the subscript k added to c.

Table 5 Accuracy of the constraint-adaptation scheme

	$p_{el}^S = 0.2$ W/cm^2		$p_{el}^S = 0.4$ W/cm^2	
	Plant optimum	Using constraint adaptation	Plant optimum	Using constraint adaptation
u_1 (mol/s)	5.438×10^{-3}	5.419×10^{-3}	1.226×10^{-2}	1.251×10^{-2}
u_2 (mol/s)	5.346×10^{-4}	5.347×10^{-4}	1.379×10^{-3}	1.378×10^{-3}
u_3 (A)	14.012	14.013	28.571	28.571
η	0.3946	0.3946	0.3016	0.3015
η_{loss}		4.37×10^{-7}		3.69×10^{-5}

For the case of a nonsquare control problem with more inputs than controlled variables, i.e., $n_u > n_{c_k} + n_h$, an additional quadratic term can be added to the MPC objective function to exploit the additional degrees of freedom towards optimality

$$J_k[\mathbf{u}(t)] = \sum_{l=D}^{p} \left\| D_l \left[\mathbf{H}(t+l|t) - \mathbf{H}^S \right] \right\|^2 + \left\| Q_{l,k} \left[\mathbf{G}_{c_k}(t+l|t) - \mathbf{G}_{c_k}^S \right] \right\|^2 + \|R_l \Delta\mathbf{u}(t+l-1)\|^2 + \|S_l \beta_k(t+l-1)\|^2 \quad (32)$$

with

$$\beta_k(t+l) = V_{k+1}^T \left[\mathbf{u}(t+l|t) - \mathbf{u}_{k+1}^* \right], \quad l = 0, \ldots, m-1 \quad (33)$$

The columns of the matrix $V_{k+1} \in \mathbb{R}^{n_u \times (n_u - n_{c_k} - n_h)}$ correspond to directions in the input space. The vector $\beta_k \in \mathbb{R}^{n_u - n_{c_k} - n_h}$ is the difference between the inputs along these directions and their optimal values. The additional term $\|S_l \beta_k(t+l-1)\|^2$ in Eq. (32) allows controlling the inputs to their optimal values along the directions given by V_{k+1}, thus addressing the $(n_u - n_{c_k} - n_h)$ residual degrees of freedom in the control problem. V_{k+1} can be selected from information given by the steady-state model used in the RTO optimization [24]. A good choice is to select directions that are tangent to the constraints $\mathbf{H}$ and $\mathbf{G}_{c_k}$ at $\mathbf{u}_{k+1}^*$. S_l is the weighting matrix on β_k.

5.2 Application to SOFC System. The same initial input and power density setpoint changes as in Sec. 4.2 are applied. Constraint adaptation and control is started at $t = 10$ min.

Since there are three input variables and one equality constraint, no more than two (independent) inequality constraints can be active simultaneously. For this SOFC system, the bounds on T_{stack} do not become active with varying power demand. Furthermore, since there is near collinearity between U_{cell}, FU, and i, these constraints are not controlled simultaneously. Hence, the quadratic objective function to be minimized by MPC can be chosen as

$$J_k[\mathbf{u}(t)] = \sum_{l=1}^{p} d^2 \left[p_{el}(t+l|t) - p_{el}^S \right]^2 + q_k^2 \left[G_{c_k}(t+l|t) - G_{c_k}^U \right]^2 + \Delta\mathbf{u}(t+l-1)^T \mathrm{R}^T \mathrm{R} \Delta\mathbf{u}(t+l-1) + \mathrm{s}^2 \beta_k(t+l-1)^2 \quad (34)$$

where G_{c_k} is a constraint that is active during the kth RTO iteration, chosen from among G_3, G_4, and G_8 in Eq. (22). The remaining degree of freedom is fixed by selecting $\mathrm{V}_{k+1} = [u_{2,k+1}^*, -u_{1,k+1}^*, 0]^{\mathrm{T}}$ [see (33)]. This choice of V_{k+1} is equivalent to fixing the excess air ratio λ_{air} to its optimal value given by constraint adaptation at iteration k.

Combination of constraint adaptation and constraint control is illustrated schematically in Fig. 7. At the kth RTO iteration, the optimal solution generated by the constraint-adaptation level is passed to the MPC level in the form of information regarding (i) the active set $\mathcal{A}_{k+1}$, which indicates the inequality constraint G_{c_k} to be controlled, and (ii) an optimal target for the additional degree of freedom, given by V_{k+1} and u_{k+1}^*.

A time step of 2 s is chosen for MPC. The step response model is obtained for $\mathbf{u} = [0.875 \times 10^{-3},\ 7.15 \times 10^{-3},\ 20.00]^{\mathrm{T}}$ and its truncation order is $n = 50$. The length of the control and prediction horizons are $m = 6$ and $p = 9$, respectively.

The performance of MPC is highly dependent on the weights chosen for the different terms in the objective function and the bounds on the input moves. These bounds for the flow rates are chosen as $\Delta u_1^{\mathrm{U}} = 5 \times 10^{-3}$ and $\Delta u_2^{\mathrm{U}} = 8.33 \times 10^{-2}$. No bound is used for the current as this would hinder quick tracking of the power density setpoint. The weighting matrix for the rate of change of the inputs is $\mathrm{R} = \mathrm{diag}(10^{-4},\ 10^{-2},\ 10^{-1})$.

For the other weights, two different cases are presented in Table 6. In case 1, tracking of the power density setpoint is favored over that of the active inequality constraint and the optimal value of the additional degree of freedom. The response is shown in Fig. 8. The power density tracking is virtually instantaneous, the power density reaches its setpoint in about 20 s. However, this aggressive policy leads to an abrupt increase of the air flow rate when the power demand is increased at $t = 70$ min, which reduces the efficiency. A less aggressive set of weights is used in case 2, for which the smoother response is shown in Fig. 9. The peaks and damped oscillations are eliminated at the expense of a slower tracking of the power density setpoint, which is now reached within 2–3 min of the change.

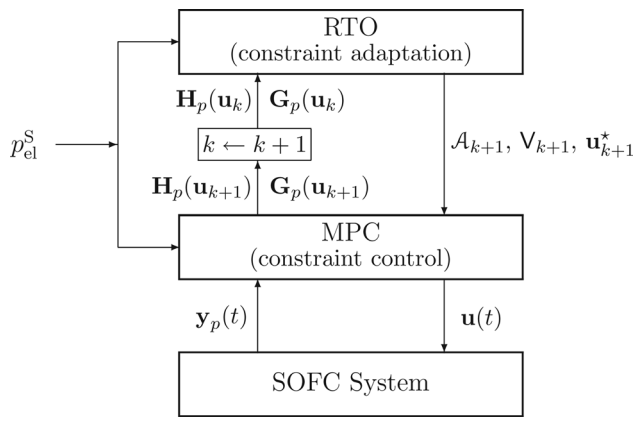

Fig. 7 Combination of constraint adaptation and constraint control

Table 6 MPC weights

	d	q	s
Case 1	5	0.005	0.01
Case 2	0.001	0.05	1

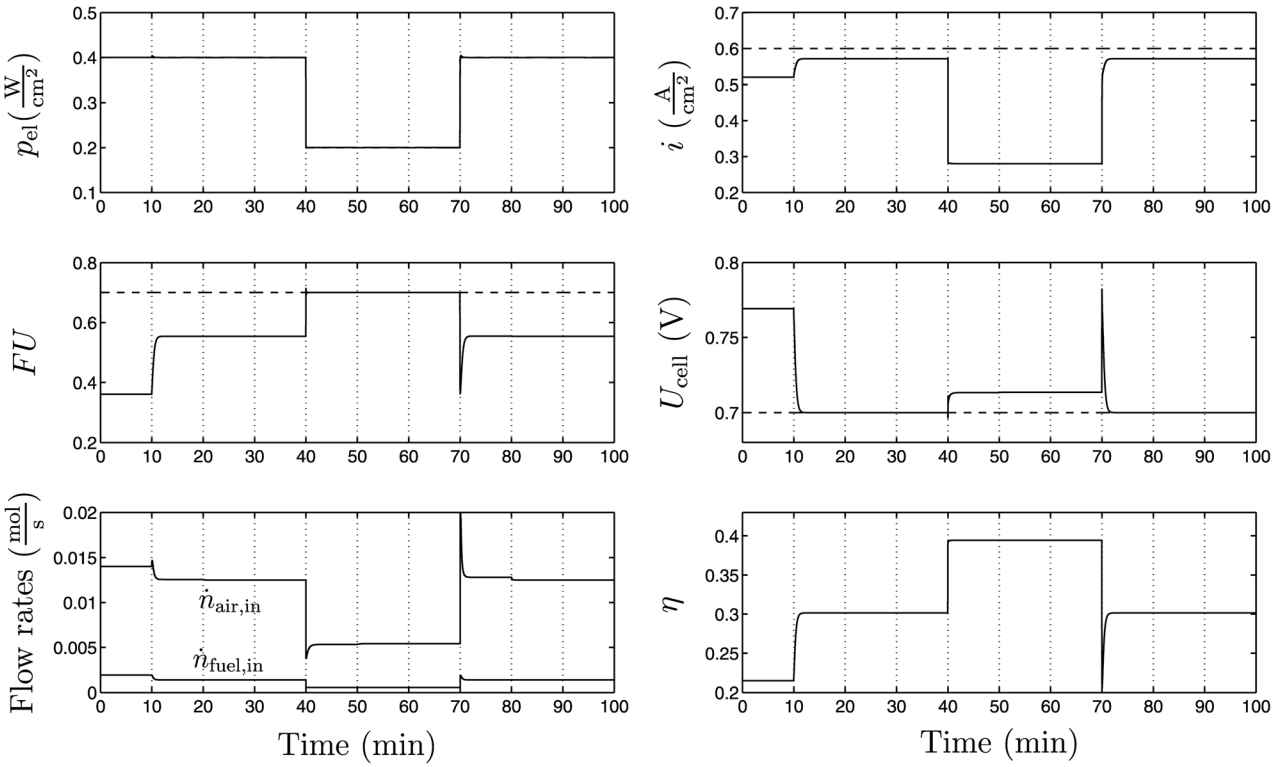

Fig. 8 Robust real-time optimization of the SOFC stack (case 1). Solid lines: performance of constraint adaptation and constraint control. Dashed lines: power density setpoint and constraint bounds. The three inputs are the flow rates $\dot{n}_{\mathrm{fuel,\,in}}$ and $\dot{n}_{\mathrm{air,\,in}}$, and the current $I = A_{\mathrm{active}}\, i$.

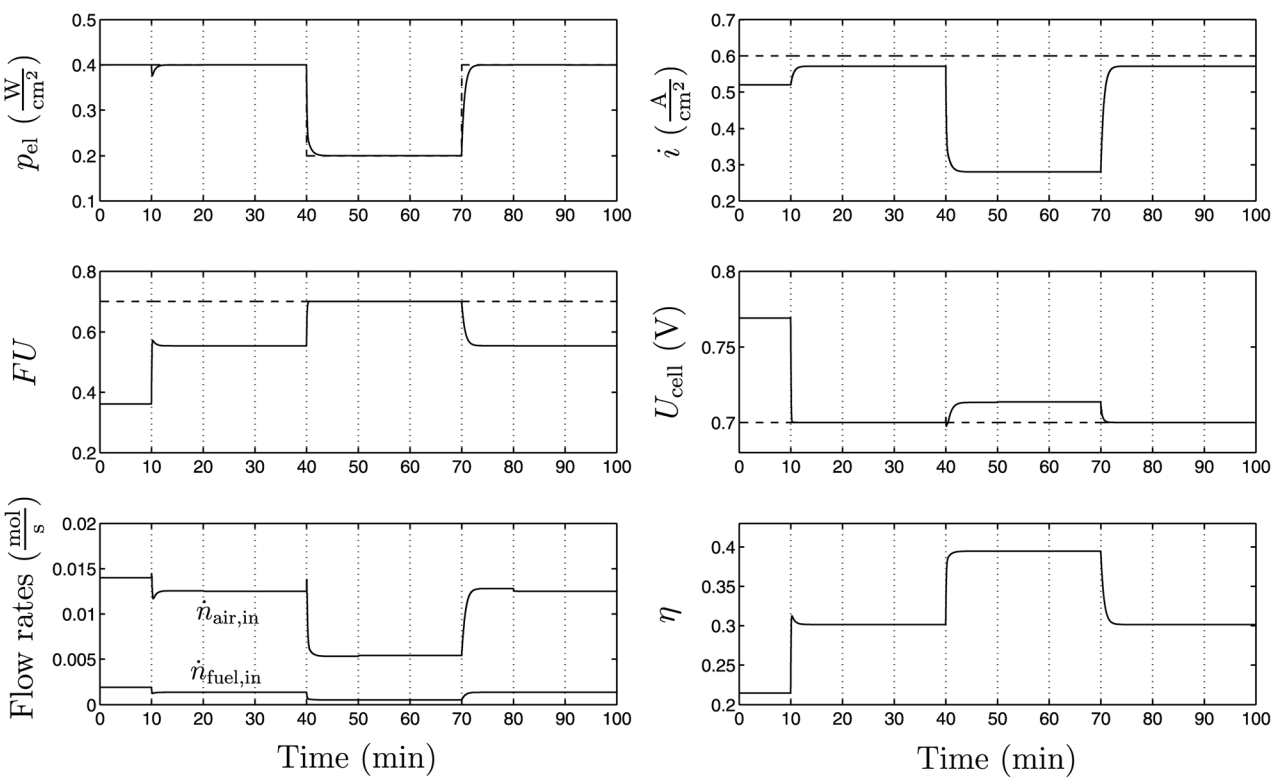

Fig. 9 Robust real-time optimization of the SOFC stack (case 2). Solid lines: performance of constraint adaptation and constraint control. Dashed lines: power density setpoint and constraint bounds. The three inputs are the flow rates $\dot{n}_{\mathrm{fuel,\,in}}$ and $\dot{n}_{\mathrm{air,\,in}}$, and the current $I = A_{\mathrm{active}}\, i$.

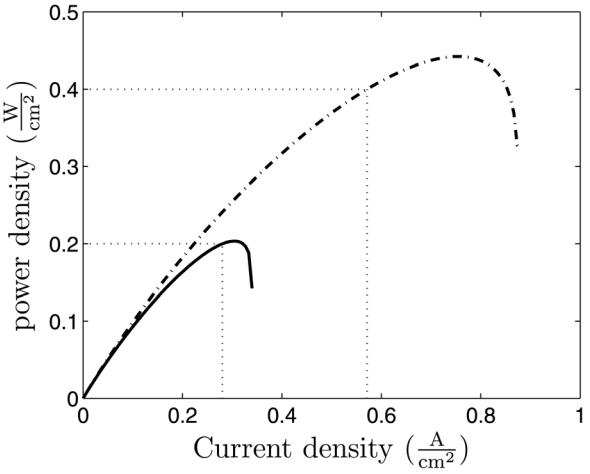

Fig. 10 Location of the optimal operating point upon convergence of the RTO-MPC scheme for the two power density setpoints of 0.2 and 0.4 W/cm^2

A comparison of Figs. 6 and 9 shows that the addition of constraint control via MPC indeed allows meeting the active constraints smoothly and efficiently. An additional advantage of combining constraint adaptation and control regards the disturbance rejection capability, as transient disturbances can be rejected by the fast inner MPC loop (Fig. 7).

5.3 Performance Curve. The power density versus current density curve is shown in Fig. 10. The location of the optimal operating points obtained upon convergence of the RTO-MPC scheme for two different power density setpoints are clearly indicated. In both cases, optimal operation is on the left side of the maximal power density. The constraints on current density, cell potential, and fuel utilization have prevented the operating point from crossing to the right of the maximal power density. Note that the step response model used by MPC was obtained on the left side of the maximal power density and thus would become inadequate if the plant operation crosses to the right side. Golbert and Lewin [2] have reported oscillatory behavior when the MPC model and the plant are on different sides of the maximal power density.

6 Conclusions

This paper has considered the real-time optimization of a simple SOFC system. A lumped dynamic model is used, which considers the electrochemical, energy and mole balances taking place inside the cell. An optimization problem has been formulated to maximize electrical efficiency at a given power demand, while respecting a number of operating constraints. It is shown that the constraints that determine optimal operation vary with the power demand. Furthermore, in the presence of model mismatch, the optimum given by the model may not provide a feasible operating point, and not even the correct set of active constraints. A control strategy combining RTO and MPC has been presented and illustrated through simulation. The strategy includes correction terms based on the difference between plant measurements and model predictions at both the RTO and MPC levels. At the RTO (steady-state optimization) level, these correction terms are used to adapt the constraints in the optimization problem, which is simpler than trying to estimate the model parameters. The MPC level is designed to implement the optimal inputs while taking care of not violating the constraints. Note that the approach can be generalized to the use of modifier adaptation instead of constraint adaptation, thereby seeking full process optimality [25]. The approach is suited for more elaborated fuel cell systems, where ensuring safety and operational constraints whilst maximizing efficiency is important. Finally, an experimental validation of the results presented in this paper has been conducted and will be available soon [26].

Nomenclature

A_{active} = active cell area (m^2)
A_{stack} = area of stack exposed to the furnace (m^2)
$c_{p,\,stack}$ = heat capacity of stack (J/kgK)
E_{act} = energy for reaction activation (J/mol)
E_{diss} = activation energy for oxygen dissociation (J/mol)
E_{elect} = activation energy for electrolyte conductivity (J/mol)
F = Faraday constant
$\mathcal{F}$ = radiative heat exchange transfer factor
FU = fuel utilization
FU_{adj} = FU adjustment factor
$\Delta G_{reaction}$ = free energy change for reaction (J/mol)
h = thickness (m)
$\Delta\dot{H}_{gases}$ = rate of enthalpy change for gases (J/s)
I = current (A)
i = current density (A/m^2)
i_0 = exchange current density (A/m^2)
k_0 = pre-exponential factor for activation overpotential
k_B = Boltzmann constant
LHV = lower heating value for H_2 (J/mol)
m_{stack} = mass of materials of stack (kg)
$\dot{n}$ = rate of molar change; molar flow rate
n_e = charge number of reaction
N_{cell} = number of cells comprising the stack
Δp = pressure loss (Pa)
P_{el} = power produced by the stack (W)
p_{el} = power density (W/m^2)
P_{blower} = power consumed by blower (W)
p = partial pressure (Pa)
p_0 = reference ambient pressure (Pa)
$\dot{Q}_{air}$ = volumetric air flow rate (m^3/s)
$\dot{Q}_{loss}$ = rate of heat loss from stack to furnace (J/s)
R = universal gas constant
R_0 = pre-exponential factor for O_2 dissociation (Ω m^2)
T = temperature (K)
U_{cell} = cell potential (V)
U_{Nernst} = Nernst potential (V)

Greek Letters

η_{act} = activation overpotential (V)
η_{diff} = diffusion overpotential (V)
η_{diss} = O_2 dissociation overpotential (V)
η_{ionic} = ionic overpotential (V)
η = SOFC efficiency
λ_{air} = excess air ratio
σ_{SB} = Stefan–Boltzmann constant
$\sigma_{0,\,elect}$ = ionic conductivity of electrolyte ($1/\Omega$ m)
ν = stoichiometric coefficient

Subscripts

an = anode
cath = cathode
cell = cell
in = inlet
out = outlet
elect = electrolyte

References

[1] Zhang, X. W., Chan, S. H., Hob, H. K., Li, J., Li, G., and Feng, Z., 2008, "Non-Linear Model Predictive Control Based on the Moving Horizon State Estimation for the Solid Oxide Fuel Cell," Int. J. Hydrogen Energy, **33**, pp. 2355–2366.
[2] Golbert, J., and Lewin, D. R., 2007, "Model-Based Control of Fuel Cells (2): Optimal Efficiency," J. Power Sources, **173**, pp. 298–309.

[3] Aguiar, P., Adjiman, C., and Brandon, N., 2005, "Anode-Supported Intermediate-Temperature Direct Internal Reforming Solid Oxide Fuel Cell II. Model-Based Dynamic Performance and Control," J. Power Sources, **147**, pp. 136–147.
[4] Golbert, J., and Lewin, D. R., 2004, "Model-Based Control of Fuel Cells: (1) Regulatory Control," J. Power Sources, **135**, pp. 135–151.
[5] Jurado, F., 2006, "Predictive Control of Solid Oxide Fuel Cells Using Fuzzy Ham-Merstein Models," J. Power Sources, **158**, pp. 245–253.
[6] Wu, X.-J., Zhu, X.-J., Cao, G.-Y., and Tu, H.-Y., 2008, "Predictive Control of SOFC Based on a GA-RBF Neural Network Model," J. Power Sources, **179**, pp. 232–239.
[7] Mueller, F., Jabbaria, F., Gaynor, R., and Brouwer, J., 2007, "Novel Solid Oxide Fuel Cell System Controller for Rapid Load Following," J. Power Sources, **172**, pp. 308–323.
[8] Marlin, T. E., and Hrymak, A. N., 1997, "Real-Time Operations Optimization of Continuous Processes," AIChE Symposium Series—CPC-V, Vol. **93**, pp. 156–164.
[9] Qin, S. J., and Badgwell, T. A., 1997, "An Overview of Industrial Model Predictive Technology," AIChE Symposium Series—CPC-V, Vol. **93**, pp. 232–256.
[10] Chachuat, B., Srinivasan, B., and Bonvin, D., 2009, "Adaptation Strategies for Real-Time Optimization," Comput. Chem. Eng., **33**, pp. 1557–1567.
[11] Maarleveld, A., and Rijnsdorp, J. E.,1970, "Constraint Control on Distillation Columns," Automatica, **6**, pp. 51–58.
[12] Chachuat, B., Marchetti, A., and Bonvin, D., 2008, "Process Optimization Via Constraints Adaptation," J. Process Contr., **18**, pp. 244–257.
[13] Forbes, J. F., and Marlin, T. E., 1994, "Model Accuracy for Economic Optimizing Controllers: The Bias Update Case," Ind. Eng. Chem. Res., **33**, pp. 1919–1929.
[14] Diethelm, S., van Herle, J., Wuillemin, Z., Nakajo, A., Autissier, N., and Molinelli, M., 2008, "Impact of Materials and Design on Solid Oxide Fuel Cell Stack Operation," J. Fuel Cell Sci. Technol., **5**(3), p. 31003.
[15] Wuillemin, Z., Autissier, N., Luong, M.-T., Van herle, J., and Favrat, D., 2008, "Modeling and Study of the Influence of Sealing on a Solid Oxide Fuel Cell," J. Fuel Cell Sci. Technol., **5**, p. 011016.
[16] Nakajo, A., Wuillemin, Z., Van herle, J., and Favrat, D., 2009, "Simulation of Thermal Stresses in Anode-Supported Solid Oxide Fuel Cell Stacks. Part I: Probability of Failure of the Cells," J. Power Sources, **193**(1), pp. 203–215.
[17] Lienhard IV, J. H., and Lienhard V, J. H., 2003, *A Heat Transfer Textbook*, 3rd ed., Phlogiston Press, Cambridge, MA.
[18] Chan, S. H., Khor, K. A., and Xia, Z. T., 2001, "A Complete Polarization Model of a Solid Oxide Fuel Cell and Its Sensitivity to Change of Cell Component Thickness," J. Power Sources, **93**, pp. 130–140.
[19] Park, J.-H., and Blumenthal, R. N., 1989, "Electronic Transport in 8 Mole Percent Y_2O_3-ZrO_2," J. Electrochem. Soc., **136**, pp. 2867–2876.
[20] Larrain, D., Van herle, J., and Favrat, D., 2006, "Simulation of SOFC Stack and Repeat Elements Including Interconnect Degradation and Anode Reoxidation Risk," J. Power Sources, **161**, pp. 392–403.
[21] Garcia, C. E., and Morari, M., 1984, "Optimal Operation of Integrated Processing Systems. Part II: Closed-Loop On-Line Optimizing Control," AIChE J., **30**(2), pp. 226–234.
[22] Maciejowski, J. M., 2002, *Predictive Control With Constraints*, Prentice-Hall, Harlow, England.
[23] Marchetti, A., 2009, "Modifier-Adaptation Methodology for Real-Time Optimization," Ph.D. thesis, No. 4449, Ecole Polytechnique Fédérale de Lausanne.
[24] Marchetti, A., Chachuat, B., and Bonvin, D., 2008, "Real-Time Optimization Via Adaptation and Control of the Constraints," 18th European Symposium on Computer Aided Process Engineering, ESCAPE Vol. 18, Lyon, France.
[25] Marchetti, A., Chachuat, B., and Bonvin, D., 2009, "Modifier-Adaptation Methodology for Real-Time Optimization," Ind. Eng. Chem. Res., **48**, pp. 6022–6033.
[26] Bunin, G., Wuillemin, Z., Francois, G., Nakajo, A., Tsikonis, L., and Bonvin, D., 2010, "Experimental Real-Time Optimization of a Solid Oxide Fuel Cell Stack Via Constraint Adaptation," 23rd International Conference on Efficiency, Cost, Optimization, Simulation and Environmental Impact of Energy Systems (ECOS 2010), Lausanne, Switzerland.